Available online at www.sciencedirect.com
ScienceDirect
Journal of Sound and Vibration 299 (2007) 229–246
JOURNAL OF SOUND AND VIBRATION
www.elsevier.com/locate/jsvi

An improved symplectic precise integration method for analysis of the rotating rigid–flexible coupled system

Yong-an Huang[a,*], Zi-chen Deng[a,b], Lin-xiao Yao[a]

[a]*Department of Engineering Mechanics, Northwestern Polytechnical University, Xi'an 710072, PR China*
[b]*State Key Laboratory of Structural Analysis of Industrial Equipment, Dalian University of Technology, Dalian 116023, PR China*

Received 15 January 2006; received in revised form 9 July 2006; accepted 18 July 2006
Available online 11 September 2006

Abstract

This paper presents an improved symplectic precise integration method (PIM) to increase the accuracy and keep the stability of the computation of the rotating rigid–flexible coupled system. Firstly, the generalized Hamilton's principle is used to establish a coupled model for the rotating system, which is discretized and transferred into Hamiltonian systems subsequently. Secondly, a suitable symplectic geometric algorithm is proposed to keep the computational stability of the rotating rigid–flexible coupled system. Thirdly, the idea of PIM is introduced into the symplectic geometric algorithm to establish a symplectic PIM, which combines the advantages of the accuracy of the PIM and the stability of the symplectic geometric algorithm. In some sense, the results obtained by this method are analytical solutions in computer for a long span of time, so the time-step can be enlarged to speed up the computation. Finally, three numerical examples show the stability of computation, the accuracy of solving stiff equations and the capability of solving nonlinear equations, respectively. All these examples prove the symplectic PIM is a promising method for the rotating rigid–flexible coupled systems.

1. Introduction

It is well known that most numerical methods, such as the traditional Runge–Kutta method (RKM), are not ideal for Hamiltonian systems, because they are not generic in the set of all dynamic systems [1]. In other words, they are not structurally stable against non-Hamiltonian perturbations. The numerical approximation by an ordinary numerical method can introduce non-Hamiltonian perturbations, which means that a Hamiltonian system will become a dissipative system when integrated by an ordinary numerical method. These two kinds of systems have completely different long-term behaviors in computational stability. Symplectic geometric algorithms (SGA) can preserve the features of Hamiltonian systems by arranging each step of the integration with the canonical or symplectic transformation.

Recently, the numerical discretization algorithms that can inherit the symplectic structure of Hamiltonian system have been studied. SGA for Hamiltonian system is firstly presented by Kang and Ruth [1,2] who have

*Corresponding author. Tel.: +86 29 88460403; fax: +86 29 88460403.
E-mail address: hyachina@yahoo.com (Y.A. Huang).

0022-460X/$ - see front matter © 2006 Elsevier Ltd. All rights reserved.
doi:10.1016/j.jsv.2006.07.009

shown that these methods can preserve Hamiltonian with high accuracy over long periods of time. It has been proven that symplectic methods with fixed step-size possess better long-term stability properties than non-symplectic methods or symplectic methods with variable step-size [3]. More comparisons between symplectic and non-symplectic algorithms can be found in Ref. [4].

Symplectic inner product is area measure which distinguishes symplectic geometry from Euclidean geometry, so it is impossible to define length by symplectic structure. Symplectic geometry can properly show the symplectic structure of Hamiltonian system, and avoid the artificially external disturbance. The solutions of Hamiltonian system are one-parameter transformations, which can inherit the symplectic structure and keep energy conservation.

So far, most applications of symplectic schemes are related to many-particle systems which are modeled as point particles. Such problems arise in astronomy and molecular dynamics [5,6]. Some results are available for the conservative rigid-body systems [7,8] and the cantilever beam and plate [9]. However, there are much few researches devoted to the rotating rigid–flexible coupled systems. In this paper, it is the first time that SGA is applied to deal with the rotating rigid–flexible coupled system.

Precise integration method (PIM) is usually utilized to solve the time-step integration for time-invariant systems. For such a problem, PIM can give highly accurate results which approach the full computer precision [10]. However, the traditional SGA cannot meet the requirements of accuracy. By introducing the idea of PIM into SGA, an improved symplectic precise integration method (SPIM) is presented to increase the accuracy of the numerical results given by SGA. SPIM is used to solve a linearly high–low frequencies system to show the accuracy, and to solve a nonlinear coupled system to indicate this method can deal with the nonlinear differential equations successfully.

The objectives of this study are that a suitable SGA is firstly applied to solve a rigid–flexible coupled system and an improved method named SPIM is established to increase the accuracy and the efficiency of SGA. This paper is organized as follows: In Section 1, the generalized Hamilton's principle is used to establish the coupled model. In Section 2, the model is transformed into Hamiltonian system to get the canonical equations. A suitable SGA is established for solving the coupled model in Section 3, and the idea of PIM is introduced into the SGA to get an improved SPIM to solve the coupled model in the next section. In the last section, three numerical simulations will be given to show the long-term stability properties of the symplectic algorithm, the high accuracy of solving stiffness equations and the powerful capability of solving nonlinear systems of SPIM, respectively.

2. A rotating flexible structure modeled by Hamilton's principle

The structure studied is shown in Fig. 1, which mainly includes a hub, a flexible tapered beam and a tip mass. The hub connects the ground with an angle spring with rigidity k_1. And the flexible beam connects the

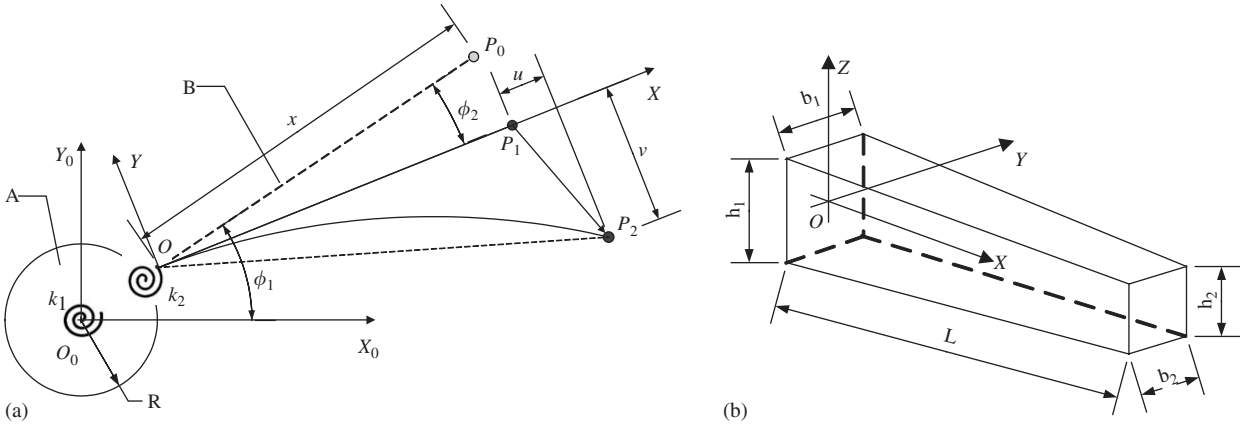

Fig. 1. A rotating rigid–flexible coupled system (a) Deformations of the rotating rigid–flexible coupled system; (b) Parameters of the tapered beam.

hub with an angle spring with rigidity k_2. The section parameters in Fig. 1(b) are b_1, h_1, b_2 and h_2. The hub's radius is R, and the tip mass is m_t.

The generalized Hamilton's principle can be written as follows:

$$\int_{t_1}^{t_2} (\delta T - \delta V + \delta W)\,\mathrm{d}t = 0, \tag{1}$$

where δT is the variation of kinetic energy, δV the variation of potential energy, δW the virtual work of external force.

In Fig. 1(a), point P_0 is moved to point P_2, and in coordination $O_0{-}X_0Y_0$ can be expressed as

$$\vec{\mathbf{R}}_{p_2} = \overrightarrow{O_0P_2} = \overrightarrow{O_0O} + \mathbf{\Phi}_1\mathbf{\Phi}_2\left(\overrightarrow{OP_1} + \overrightarrow{P_1P_2}\right) = \vec{\mathbf{R}} + \mathbf{\Phi}_1\mathbf{\Phi}_2\begin{bmatrix} x + u(x,t) \\ v(x,t) \end{bmatrix}, \tag{2}$$

where $\vec{\mathbf{R}} = \overrightarrow{O_0O}$ is the position of the origin O of coordination $O{-}XY$ in coordination $O_0{-}X_0Y_0$. $\overrightarrow{OP_1}$, written as $[x,0]^{\mathrm{T}}$, is the position of point P_1 in coordination $O{-}XY$ before deforming. $\overrightarrow{P_1P_2}$ is the deformation vector $[u(x,t),\ v(x,t)]^{\mathrm{T}}$, can be written in details as follows:

$$\overrightarrow{P_1P_2} = \begin{bmatrix} u(x,t) \\ v(x,t) \end{bmatrix} = \begin{bmatrix} w_1(x,t) + w_c(x,t) \\ w_2(x,t) \end{bmatrix} = \begin{bmatrix} w_1(x,t) + \frac{1}{2}\int_0^x \left(\dfrac{\partial w_2(\xi,t)}{\partial \xi}\right)^2 \mathrm{d}\xi \\ w_2(x,t) \end{bmatrix}, \tag{3}$$

where $w_1(x,t)$ is the axial extension quantity, and $w_2(x,t)$ the transverse displacement. $w_c(x,t)$ is the axial shrinking quantity caused by the transverse displacement $w_2(x,t)$. $\mathbf{\Phi}_1$ is the transformation matrix of the hub correspond to the coordination $O_0{-}X_0Y_0$, and $\mathbf{\Phi}_2$ is the coordination $O{-}XY$ correspond to the hub. These matrixes can be expressed as

$$\mathbf{\Phi}_2 = \begin{bmatrix} \cos\phi_2 & -\sin\phi_2 \\ \sin\phi_2 & \cos\phi_2 \end{bmatrix} \quad \text{and} \quad \mathbf{\Phi}_1 = \begin{bmatrix} \cos(\phi_1) & -\sin(\phi_1) \\ \sin(\phi_1) & \cos(\phi_1) \end{bmatrix}. \tag{4}$$

The total kinetic energy is

$$T = \frac{1}{2}J_A\dot{\phi}_1^2 + \frac{1}{2}\int_0^L \rho A(x)\dot{\vec{\mathbf{R}}}_{P_2}^{\mathrm{T}}\dot{\vec{\mathbf{R}}}_{P_2}\,\mathrm{d}x, \tag{5}$$

where J_A is the rotary inertia of the hub, and the area $A(x)$ is function of x, and L and ρ are the length and the density of the flexible beam.

The total potential energy is

$$V = \frac{1}{2}k_1\phi_1^2 + \frac{1}{2}k_2\phi_2^2 + \frac{1}{2}\int_0^L EA(x)(u'(x,t))^2\,\mathrm{d}x + \frac{1}{2}\int_0^L EI(x)(v''(x,t))^2\,\mathrm{d}x + \frac{1}{2}\int_0^L f(x)v'^2\,\mathrm{d}x, \tag{6}$$

where $f(x)$ is centrifugal force, the moment of inertia $I(x)$ is function of x, and E is the Young's modulus of the beam.

The beam is divided into n elements with the same length, which is shown in Fig. 2.

The point in the ith element can be expressed in the reference coordination $O{-}XY$ as follows:

$$x = L_i + \bar{x}, \tag{7}$$

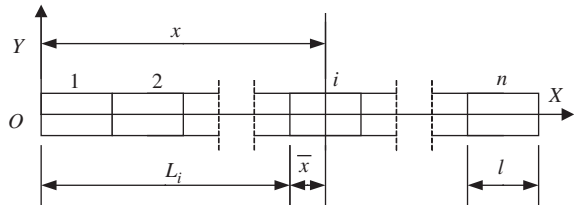

Fig. 2. The finite element model of the tapered beam.

where

$$L_i = \frac{(i-1)}{n} L.$$

Since the axial extensions, the transverse and the slope displacements of the beam can be regarded as generalized variables, the deformations u and v in the ith element are expressed herein as the interpolation of the two nodes coordinates of this element using an element shape function, given by

$$u = \mathbf{N}_u \mathbf{q}^i, \;\; v = \mathbf{N}_v \mathbf{q}^i, \;\; u^t = \mathbf{N}_u^t \mathbf{q}^t, \;\; v^t = \mathbf{N}_v^t \mathbf{q}^t, \tag{8}$$

where $\mathbf{N}_u$ and u are the axial displacement shape function and the axial extension, respectively. $\mathbf{N}_v$ and v are the transverse displacement shape function and the transverse displacement, respectively. Superscript t denotes the tip mass. These shape functions can be seen in Ref. [11].

Displacement vectors $\mathbf{q}^i$ and $\mathbf{q}^t$ can be written as

$$\mathbf{q}^i = \left[u^i, v^i, \theta^i, u^{i+1}, v^{i+1}, \theta^{i+1}\right], \tag{9}$$

$$\mathbf{q}^t = \left[u^n, v^n, \theta^n, u^{n+1}, v^{n+1}, \theta^{n+1}\right], \tag{10}$$

where θ^i is the slope angle displacement, respectively. And we can get

$$u' = \mathbf{N}_u' \mathbf{q}^i, \dot{u} = \mathbf{N}_u \dot{\mathbf{q}}^i, \tag{11}$$

$$v' = \mathbf{N}_v' \mathbf{q}^i, \;\; v'' = \mathbf{N}_v'' \mathbf{q}^i, \;\; \dot{v} = \mathbf{N}_v \dot{\mathbf{q}}^i. \tag{12}$$

Then we can get the deformation vector in coordination $O{-}XY$ as follows:

$$\mathbf{r}_2 = \begin{bmatrix} u(L_i + \bar{x}, t) \\ v(L_i + \bar{x}, t) \end{bmatrix} = \begin{bmatrix} \mathbf{N}_u \mathbf{q}^i \\ \mathbf{N}_v \mathbf{q}^i \end{bmatrix}. \tag{13}$$

Lagrangian can be gained by Eqs. (7)–(13). By the use of finite element method, the discretized Lagrangian can be written as

$$\begin{aligned} \Psi = T - V = {} & \frac{1}{2} J_A \dot{\phi}_1^2 + \frac{1}{2} \int_0^L \rho A(x) \left(((R + \bar{x} + u)\dot{\theta} + \dot{v})^2 + (v\dot{\theta} - \dot{u})^2 \right) \mathrm{d}\bar{x} \\ & + \frac{1}{2} m_t \left(((R + L + u_t)\dot{\theta} + \dot{v}_t)^2 + (v_t \dot{\theta} - \dot{u}_t)^2 \right) \dot{\vec{\mathbf{R}}}_t^{\mathrm{T}} \dot{\vec{\mathbf{R}}}_t \\ & - \frac{1}{2} k_1 \phi_1^2 - \frac{1}{2} k_2 \phi_2^2 - \frac{1}{2} \int_0^L \left(EA(\bar{x}) u'^2 + EI(\bar{x}) v''^2 + f(\bar{x}) v'^2 \right) \mathrm{d}\bar{x}. \end{aligned} \tag{14}$$

Then we can get the dynamic equation of the vibration of the flexible beam according to the local float coordination by virtue of the generalized Hamilton's principle

$$\begin{bmatrix} \mathbf{M}_{mm} & 0 \\ 0 & \mathbf{M}_{\phi\phi} \end{bmatrix} \begin{bmatrix} \ddot{\mathbf{q}} \\ \ddot{\mathbf{\Phi}} \end{bmatrix} + \begin{bmatrix} \mathbf{C}_{mm} & \mathbf{C}_{m\phi} \\ \mathbf{C}_{\phi m} & \mathbf{C}_{\phi\phi} \end{bmatrix} \begin{bmatrix} \dot{\mathbf{q}} \\ \dot{\mathbf{\Phi}} \end{bmatrix} + \begin{bmatrix} \mathbf{K}_{mm} & \mathbf{K}_{m\phi} \\ \mathbf{K}_{\phi m} & \mathbf{K}_{\phi\phi} \end{bmatrix} \begin{bmatrix} \mathbf{q} \\ \mathbf{\Phi} \end{bmatrix} = \begin{bmatrix} \mathbf{F}_m \\ \mathbf{F}_\phi \end{bmatrix}, \tag{15}$$

where $\mathbf{\Phi} = [\phi_1, \phi_2]^{\mathrm{T}}$. It can be noted there are coupled terms between the transverse displacements, the axial extensions and the rigid rotations. Since the rotating of the structure, there are additional damp terms and stiffness terms in Eq. (15). Considering the effect of the non-uniform section, the area $A(x)$ must be placed in the integral expression, and cannot deal with it as a constant. Though the tapered beam is more difficult than the uniform beam, it is closer to the real structure.

3. Canonical equation for Hamiltonian vibration systems

The generalized displacement vector is defined as

$$\mathbf{y} = \begin{bmatrix} \mathbf{q} \\ \mathbf{\Phi} \end{bmatrix}. \tag{16}$$

The generalized momentum is defined as

$$\mathbf{p}(t) = \frac{\partial L(\mathbf{y}, \dot{\mathbf{y}}, t)}{\partial \dot{\mathbf{y}}} = \mathbf{M}(t)\dot{\mathbf{y}}. \tag{17}$$

By Legendre transformation, Hamiltonian can be gained

$$H(\mathbf{p}, \mathbf{y}, t) = \mathbf{p}^{\mathrm{T}}(t)\dot{\mathbf{y}}(t) - L(\mathbf{y}, \dot{\mathbf{y}}, t) = T(\mathbf{p}, \mathbf{y}, t) + V(\mathbf{y}, t) = \tfrac{1}{2}\mathbf{p}^{\mathrm{T}}(t)\mathbf{M}^{-1}(\mathbf{y}, t)\mathbf{p}(t) + V(\mathbf{y}, t). \tag{18}$$

The canonical equations can be gained

$$\dot{\mathbf{y}} = \frac{\partial H}{\partial \mathbf{p}} = \mathbf{H}_p, \quad \dot{\mathbf{p}} = -\frac{\partial H}{\partial y} = \mathbf{H}_y, \tag{19}$$

$$\frac{\partial L}{\partial t} = -\frac{\partial H}{\partial t}, \tag{20}$$

where the generalized displacement vector $\mathbf{y} = [q_1(t)\ q_2(t) \ldots q_n(\mathrm{t})\ \phi_1(t)\ \phi_2(t)]^{\mathrm{T}}$, the generalized momentum vector $\mathbf{p} = [p_1(t)\ p_2(t) \ldots p_n(\mathrm{t})\ p_{n+1}(t)\ p_{n+2}(t)]^{\mathrm{T}}$, and

$$\mathbf{H}_y = \left[\frac{\partial H}{\partial q_1}\frac{\partial H}{\partial q_2} \cdots \frac{\partial H}{\partial q_n}\frac{\partial H}{\partial \phi_1}\frac{\partial H}{\partial \phi_2}\right]^{\mathrm{T}}, \quad \mathbf{H}_p = \left[\frac{\partial H}{\partial p_1}\frac{\partial H}{\partial p_2} \cdots \frac{\partial H}{\partial p_n}\frac{\partial H}{\partial p_{\phi 1}}\frac{\partial H}{\partial p_{\phi 2}}\right]^{\mathrm{T}}$$

more about the Hamiltonian system can be seen in Ref. [12].

Considering the mass matrix as the function of the generalized displacements $\mathbf{y}$, we can get

$$\mathbf{M}_y = \left[\frac{\partial M}{q_1}\frac{\partial M}{q_2} \cdots \frac{\partial M}{q_n}\frac{\partial M}{\phi_1}\frac{\partial M}{\phi_2}\right]. \tag{21}$$

Then

$$\left[\frac{\partial \mathbf{M}}{q_1}\mathbf{H}_p\frac{\partial \mathbf{M}}{q_2}\mathbf{H}_p \cdots \frac{\partial \mathbf{M}}{q_n}\mathbf{H}_p\frac{\partial \mathbf{M}}{\phi_1}\mathbf{H}_p\frac{\partial \mathbf{M}}{\phi_2}\mathbf{H}_p\right] = \mathbf{M}_y(\mathbf{I} \otimes \mathbf{H}_p) \stackrel{\mathrm{def}}{=} \mathbf{A}, \tag{22}$$

where $\mathbf{I} \in \mathbf{R}^{(n+2)\times(n+2)}$ is an identity matrix, $\otimes$ denotes Kronecker inner product. Then the canonical form can be transformed into

$$\dot{\mathbf{y}} = \mathbf{H}_p = \mathbf{M}^{-1}\mathbf{p}, \ \ \dot{\mathbf{p}} = -\mathbf{H}_y = \frac{1}{2}\mathbf{A}^{\mathrm{T}}\mathbf{H}_p - \frac{\partial V}{\partial y}. \tag{23}$$

4. Symplectic Runge–Kutta method for vibration systems

To discover the mathematic geometric characteristic of Hamiltonian canonical equations, Eq. (4) needs writing in matrix form. By introducing the states vector $\mathbf{z} = [y_1, y_2, \ldots, y_{n+2}, p_1, p_2, \ldots, p_{n+2}]$, Eq. (4) can be expressed as follows:

$$\dot{\mathbf{z}} = \mathbf{J}_{2n}\mathbf{H}_z = f(\mathbf{z}), \tag{24}$$

where

$$J_{2(n+2)} = \begin{bmatrix} 0 & -I_{n+2} \\ I_{n+2} & 0 \end{bmatrix}$$

is an identity symplectic matrix, and $\mathbf{I}_{n+2}$ is an identity matrix, and more about it can be found in Ref. [7].

There are two main ways to establish SGA for Hamiltonian systems, which are generating functions method and directly symplectic Runge–Kutta method (SPKM). An sth-order SPKM is designed in detail as follows:

$$\mathbf{z}_{k+1} = \mathbf{z}_k + h\sum_{i=1}^{s} b_i f(\mathbf{Y}_i), \tag{25}$$

$$\mathbf{Y}_i = \mathbf{z}_k + h\sum_{j=1}^{s} a_{ij} f(\mathbf{Y}_j) \quad (i \leqslant i \leqslant s), \tag{26}$$

where $h = t_{k+1} - t_k (k \geqslant 0)$.

Let $\mathbf{\Omega} = [m_{ij}]$ be a real $s \times s$ matrix given by

$$\mathbf{\Omega} = \mathbf{BA} + \mathbf{A}'\mathbf{B} - \mathbf{bb}', \tag{27}$$

where $\mathbf{A} = (a_{ij})$, $\mathbf{b} = [b_i]$, and define $\mathbf{B} = \mathrm{diag}[b_i]$. For $i,j = 1,\ldots,s$, the matrix $\mathbf{\Omega}$ comes up frequently in the study of Runge–Kutta schemes and nonlinear stability [12,13], and moreover Lasagni, Sanz–Serna and Suris showed that

Theorem 1. *If $\mathbf{\Omega} = 0$, then the corresponding implicit RKM is symplectic.*

In this paper, the 2nd-order accuracy form is adopted to generate the symplectic Runge–Kutta algorithm:

$$\mathbf{A} = \begin{bmatrix} \frac{1}{4} & 0 \\ \frac{1}{2} & \frac{1}{4} \end{bmatrix}, \quad \mathbf{b} = \begin{bmatrix} \frac{1}{2} \\ \frac{1}{2} \end{bmatrix}, \tag{28}$$

$$\mathbf{z}_{k+1} = \mathbf{z}_k + \frac{h}{2}(f(\mathbf{Y}_1) + f(\mathbf{Y}_2)), \tag{29}$$

$$\begin{bmatrix} \mathbf{Y}_1 \\ \mathbf{Y}_2 \end{bmatrix} = \begin{bmatrix} \mathbf{z}_k + \frac{h}{2} f(\mathbf{Y}_1) \\ \mathbf{z}_k + \frac{h}{2} f(\mathbf{Y}_1) + \frac{h}{4} f(\mathbf{Y}_2) \end{bmatrix}. \tag{30}$$

The above algorithm is a time-centered scheme.

5. Symplectic precise integration method

PIM used to solve the time-step integration for the time-invariant systems, which gives highly precise numerical results approaching the full computer precision [10], so it is suitable for solving stiffness equations. But the traditional PIM is effective for linear systems. In this paper, the idea of PIM is introduced into SGA to establish SPIM which inherits properties of SGA and PIM.

How to calculate the exponential matrix $\exp(\mathbf{Ax})$ plays an important role in dynamic simulations. There are many ways to get its numerical value, such as *Padé* approximants, Taylor expansion, which are the initial idea of PIM. In this paper, the idea of PIM is introduced into the SGA to establish SPIM, and it will be proven that the accuracy and the efficiency of the new algorithm is better than that of the traditional SGA and the traditional RKM by two numerical examples.

Discussions on time-invariant systems or linear systems can be found in Ref. [10], and the time-variant systems or nonlinear systems have been studied by the author [14]. But all these studies are devoted to

non-symplectic algorithms. So it is important and necessary to discuss how to establish SPIM and what advantages it has.

The nonlinearly coupled equations can be written as

$$\mathbf{J}_{2(n+2)}\mathbf{H}_z = \mathbf{H}_0\mathbf{z} + \mathbf{H}_1(\mathbf{z}), \tag{31}$$

where $\mathbf{H}_0$ is a constant matrix, $\mathbf{H}_1(\mathbf{z})$ is a time-variant matrix or related to the states vector. $\mathbf{H}_1(\mathbf{z})$ can be seen as the external force vector, then Eq. (24) can be written as

$$\dot{\mathbf{z}} = \mathbf{H}_0\mathbf{z} + \mathbf{H}_1(\mathbf{z}). \tag{32}$$

In time span (t_k, t_{k+1}), matrix $\mathbf{H}_1(\mathbf{z})$ can be treated as

$$\mathbf{H}_1(\mathbf{z}) = \mathbf{r}_0 + \mathbf{r}_1(t - t_k). \tag{33}$$

The solution of equation $\dot{\mathbf{z}} = \mathbf{H}_0\mathbf{z}$ can be written as

$$\mathbf{z} = \exp(\mathbf{H}_0 \cdot t) \cdot \mathbf{z}_0. \tag{35}$$

Supposed that $\mathbf{z} = \mathbf{z}_k$ at time t_k,

$$\exp(\mathbf{H} \cdot \tau) = \left[\exp(\mathbf{H} \cdot \tau/m)\right]^m, \tag{36}$$

where m is an arbitrary integer. It is suggested to let $m = 2^N$, such as $N = 20$, $m = 1{,}048{,}576$. Since τ is a short time, $\Delta t = \tau/m$ is a shorter time. And we can get

$$\begin{aligned}
\exp(\mathbf{H} \cdot \tau) &= [\exp(\mathbf{H} \cdot \Delta t)]^m = [\exp(\mathbf{H} \cdot \Delta t)]^{2^N} \\
&= [\exp(\mathbf{H} \cdot \Delta t)]^{2^{(N-1)}} \times [\exp(\mathbf{H} \cdot \Delta t)]^{2^{(N-1)}} \\
&\approx [\mathbf{I} + \mathbf{T}_a]^{2^{(N-1)}} \times [\mathbf{I} + \mathbf{T}_a]^{2^{(N-1)}} \\
&= \left([\mathbf{I} + \mathbf{T}_a]^{2^{(N-2)}} \times [\mathbf{I} + \mathbf{T}_a]^{2^{(N-2)}}\right) \times \left([\mathbf{I} + \mathbf{T}_a]^{2^{(N-2)}} \times [\mathbf{I} + \mathbf{T}_a]^{2^{(N-2)}}\right),
\end{aligned} \tag{37}$$

where

$$\mathbf{T}_a = \mathbf{H}\Delta t + \frac{(\mathbf{H}\Delta t)^2}{2} + \frac{(\mathbf{H}\Delta t)^3}{3!} + \frac{(\mathbf{H}\Delta t)^4}{4!}.$$

Eq. (37) can be get by the following code for $(i = 1;1 <= N;\mathrm{i}++)$ $\{\mathbf{T}_a = 2\mathbf{T}_a + \mathbf{T}_a \times \mathbf{T}_a\}$.

When the computation is over, the transfer function can be gained as

$$\mathbf{\Psi}(t) = \mathbf{I} + \mathbf{T}_a. \tag{38}$$

The traditional PIM is not suitable for solving the Hamiltonian problems, which is just a non-symplectic geometric algorithm with higher accuracy, so it is not a perfect scheme for Hamiltonian system.

The most important problem of PIM applied in Hamiltonian systems is how to calculate transformation matrix $\exp(H \cdot \tau)$ and preserve the symplectic structure of Hamiltonian systems. Herein, the *Padé* approach is adopted, so $\exp(H \cdot \tau)$ can be expressed as

$$\exp(\mathbf{H} \cdot \tau) \approx \frac{n_{lm}(\mathbf{H} \cdot \tau)}{d_{lm}(\mathbf{H} \cdot \tau)} = \mathbf{\Psi}_{lm}(\mathbf{H} \cdot \tau), \tag{39}$$

where

$$n_{lm}(\mathbf{H} \cdot \tau) = \sum_{k=0}^{m} \frac{(l+m-k)!m!}{(l+m)!k!(m-k)!}(\mathbf{H} \cdot \tau)^k, \quad d_{lm}(\mathbf{H} \cdot \tau) = \sum_{k=0}^{m} \frac{(l+m-k)!m!}{(l+m)!k!(m-k)!}(-H \cdot \tau)^k.$$

Theorem 2. *If* $\mathbf{H}$ *is an infinitesimal symplectic operator, and* $|t|$ *is small enough, then* $\mathbf{\Psi}_{lm}(\mathbf{H} \cdot \tau)$ *is symplectic matrix. If and only if* $l = m$, $\mathbf{\Psi}_{ll}(x)$ *is a Padé diagonal approach.*

In order to illuminate SPIM conveniently, we select $l = 2$, $m = 2$, then the following can be gained:

$$\mathbf{z}_{n+1} = \mathbf{z}_n + \frac{\tau\mathbf{H}}{2}(\mathbf{z}_n + \mathbf{z}_{n+1}) + \frac{\tau^2\mathbf{H}^2}{12}(\mathbf{z}_n - \mathbf{z}_{n+1}) \tag{40}$$

and the transformation function can be expressed as follows:

$$\mathbf{z}_{n+1} = \mathbf{\Psi}_{22}(\mathbf{H}\cdot\tau)\mathbf{z}_n, \tag{41}$$

where

$$\mathbf{\Psi}_{22}(\mathbf{H}\cdot\tau) = \frac{\mathbf{I} + \dfrac{\mathbf{H}\cdot\tau}{2} + \dfrac{(\mathbf{H}\cdot\tau)^2}{12}}{\mathbf{I} - \dfrac{\mathbf{H}\cdot\tau}{2} + \dfrac{(\mathbf{H}\cdot\tau)^2}{12}}.$$

This method achieves 4th-order accuracy:

$$\begin{aligned}\exp(\mathbf{H}\cdot\tau) &= \left[\exp(\mathbf{H}\cdot\tau/m)\right]^m = \mathbf{\Psi}(\mathbf{H}\cdot\tau/m)^m \\ &\approx \left[\frac{\mathbf{I} + \dfrac{\mathbf{H}\cdot\tau/m}{2} + \dfrac{(\mathbf{H}\cdot\tau/m)^2}{12}}{I - \dfrac{\mathbf{H}\cdot\tau/m}{2} + \dfrac{(\mathbf{H}\cdot\tau/m)^2}{12}}\right]^{2^N} = \frac{(\mathbf{I}+\mathbf{T}_a)^{2^{(N-1)}}(\mathbf{I}+\mathbf{T}_a)^{2^{(N-1)}}}{(\mathbf{I}+\mathbf{T}_b)^{2^{(N-1)}}(\mathbf{I}+\mathbf{T}_b)^{2^{(N-1)}}},\end{aligned} \tag{42}$$

where

$$\mathbf{T}_a = \frac{\mathbf{H}\tau/m}{2} + \frac{(\mathbf{H}\tau/m)^2}{12}, \quad \mathbf{T}_b = -\frac{\mathbf{H}\tau/m}{2} + \frac{(\mathbf{H}\tau/m)^2}{12}.$$

If $\mathbf{T}_a$ are arbitrary, then

$$(\mathbf{I}+\mathbf{T}_a)\times(\mathbf{I}+\mathbf{T}_a) = \mathbf{I} + 2\mathbf{T}_a + \mathbf{T}_a\times\mathbf{T}_a, \tag{43}$$

where matrixes $\mathbf{T}_a$ are very small. In the computation, one of the most important points is that only the additional matrix $\mathbf{T}_a$ of Eq. (43) should be kept in the memory rather than the matrix $\mathbf{T} = (\mathbf{I}_n + \mathbf{T}_a + \mathbf{T}_a\times\mathbf{T}_a)$. Because $2\mathbf{T}_a$ and $\mathbf{T}_a\times\mathbf{T}_a$ are extremely small (fine scale). If they are added to the identity matrix $\mathbf{I}_n$ (coarse scale), they will become appended parts, and their precision will be seriously dropped in the round-off operation in computer operation, in fact $\mathbf{T}_a$ and $\mathbf{T}_a\times\mathbf{T}_a$ are incremental parts. Eq. (39) can be realized by the following code for $(i = 1;1 <= N;i++)$ $\{\mathbf{T}_a = 2\mathbf{T}_a + \mathbf{T}_a\times\mathbf{T}_a;\ \mathbf{T}_b = 2\mathbf{T}_b + \mathbf{T}_b\times\mathbf{T}_b;\}$.

So Eq. (39) can be written as

$$\mathbf{\Psi}(\mathbf{H}\cdot\tau) = \frac{\mathbf{I}+\mathbf{T}_a}{\mathbf{I}+\mathbf{T}_b}. \tag{44}$$

If the linear interpolation approximation is used in the interval $\mathbf{T}_k \sim \mathbf{T}_{k+1}$, the solution of the nonlinear system can be written as

$$\mathbf{z}_{k+1} = \mathbf{\Psi}\left[\mathbf{z}_k + \mathbf{H}^{-1}\left(\mathbf{r}_0 + \mathbf{H}^{-1}\mathbf{r}_1\right)\right] - \mathbf{H}^{-1}\left[\mathbf{r}_0 + \mathbf{H}^{-1}\mathbf{r}_1 + \mathbf{r}_1\tau\right]. \tag{45}$$

However, the linear interpolation is a rough approximation, and there are lots of different approximation methods. The nonlinear part $\mathbf{H}(\mathbf{z})$ can be approximated by the following functions:

(1) Explicit method, such as linear interpolation, polynomials, trigonometric functions, and the product of these functions, etc. The linear interpolation approximation can be expressed as follows:

$$\mathbf{r}_0 = \mathbf{H}_1(\mathbf{z}_k, t_k), \quad \mathbf{r}_1 = \mathbf{H}_1'(\mathbf{z}_k, t_k). \tag{46}$$

(2) Implicit method, such as predictor correcting method. $\mathbf{r}_1$ can be calculated by the following two steps: (1) predicting, $\tilde{\mathbf{z}}_{k+1} = \mathbf{H}(\mathbf{z}_k, t_k)$; (2) correcting, $\mathbf{z}_{k+1} = \tilde{\mathbf{H}}(\mathbf{z}_k, \tilde{\mathbf{z}}_{k+1}, t_k, t_{k+1})$.

Then $\mathbf{r}_1$ can be written as

$$\mathbf{r}_1 = \frac{\mathbf{H}(\mathbf{z}_{k+1}, t_{k+1}) - \mathbf{H}(\mathbf{z}_k, t_k)}{t_{k+1} - t_k}. \tag{47}$$

Remark 1. Eq. (47) can be integrated analytically in computer.

6. Numerical examples

In this section, three examples are adopted to show advantages of SGA and SPIM in different sides, such as the long-term stability of symplectic algorithm, the high accuracy of solving stiff equations, and the capability of solving nonlinear systems of SPIM, respectively. Structures of these examples can be abstracted from the structure shown in Fig. 1.

6.1. Overall rotational cantilever beam—the stability of computation

Supposed the rigid radius is $R = 0$, and angle springs are $k_1 = 0$, $k_2 = +\infty$, and the tip mass is $m_t = 0.085\,\text{kg}$. Then we can get a coupled structure of hub and tapered beam with tip mass which is usually studied in multibody field. Parameters of the hub and tapered beam with tip mass structure are listed as follows: The length is $L = 8\,\text{m}$; the density is $\rho = 2.7667 \times 10^3\,\text{kg/m}^3$; the Young's modulus is $E = 6.8952 \times 10^{10}\,\text{N/m}^2$; and the section parameters are $b_1 = 0.04596\,\text{m}$, $h_1 = 0.00248\,\text{m}$, $b_2 = 0.02673\,\text{m}$, $h_2 = 0.00144\,\text{m}$, respectively. The area $\mathbf{A}(x)$ and the inertia moment $\mathbf{I}(x)$ can be calculated by parameters b_1, h_1, b_2 and h_2 (Fig. 3).

Since the set of differential equations are very stiff, it is very strict with time-step in solving this equation. Two time-steps involved in this example are 0.0001 and 0.0005, respectively. And the initial states vector are $\mathbf{z}_0 = [0,0.1,0.5,0,0.2,1,0,0,0,0,0,0,0,0]$. In this paper, only axial vibration is analyzed and shown in Figs. 4 and 5. And the calculated results of total energy are plotted in Figs. 6–9.

In all these results, methods adopted are the 2nd-order implicit SGA and the 4th-order RKM, respectively. The results in Figs. 4–7 are calculated with time-step 0.0001.

The result in Fig. 4 is calculated by the 2nd-order implicit symplectic RKM which is a kind of SGA, and the result in Fig. 5 is calculated by the traditional RKM. From Figs. 4 and 5, it can be found the difference in amplitudes of states of the two methods. The amplitude in Fig. 4 keeps constant, however, that in Fig. 5 decreases gradually. All these indicate there is energy dissipation in the traditional RKM, but SGA is an energy conservation method. In other words, SGA is a structure-persevered method, which can keep the stability of the results in long periods of time.

The total energies calculated by SGA and RKM are plotted in Figs. 6 and 7, respectively. From Fig. 6, it can be observed that the total energy waves in a certain amplitude, and does not decrease with time. But the energy given by RKM departs from the original energy gradually.

From above, we can observe that SGA is better than RKM in long-time simulation and SGA can keep the conservation of the total mechanical energy, but RKM cannot. It can be inferred that the energy calculated by

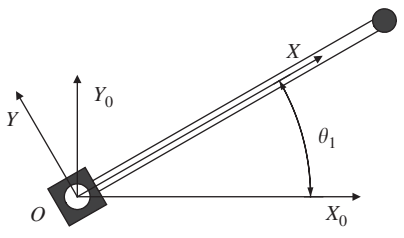

Fig. 3. A cantilever beam with rotating base.

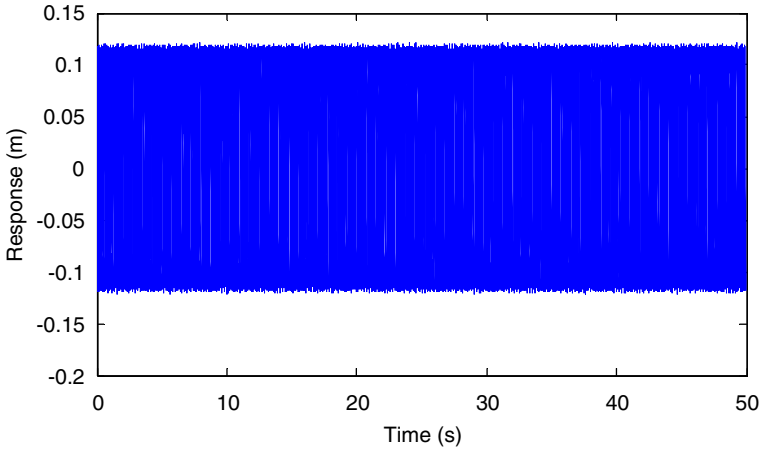

Fig. 4. The result simulated by SRKM algorithm with step-size 0.0001.

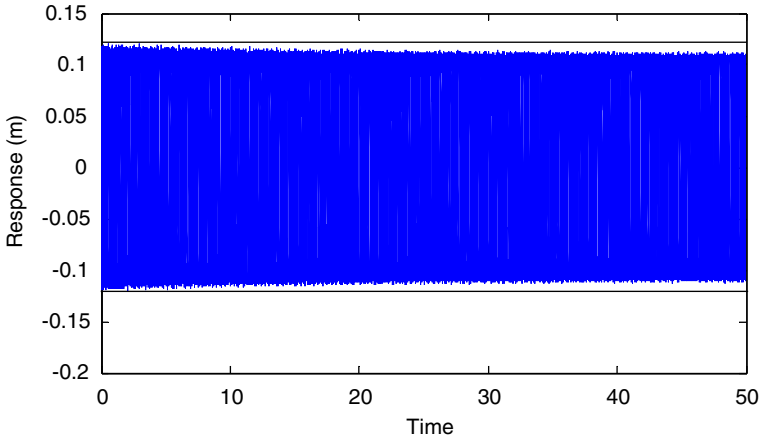

Fig. 5. The result simulated by RKM algorithm with step-size 0.0001.

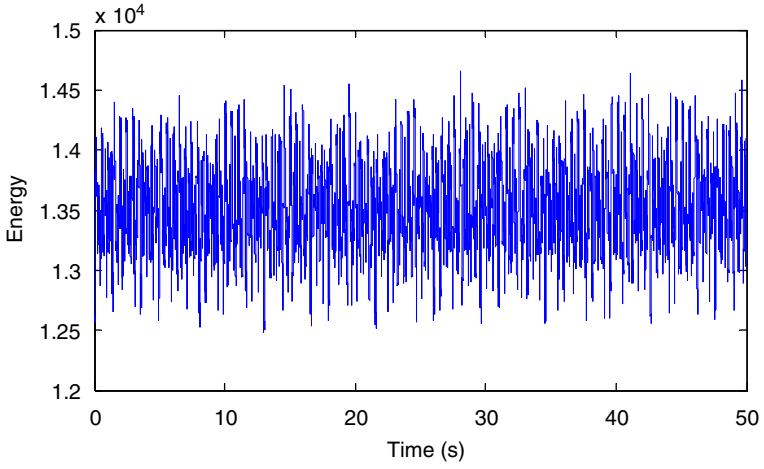

Fig. 6. The total energy of the system computed by SRKM with step-size 0.0001.

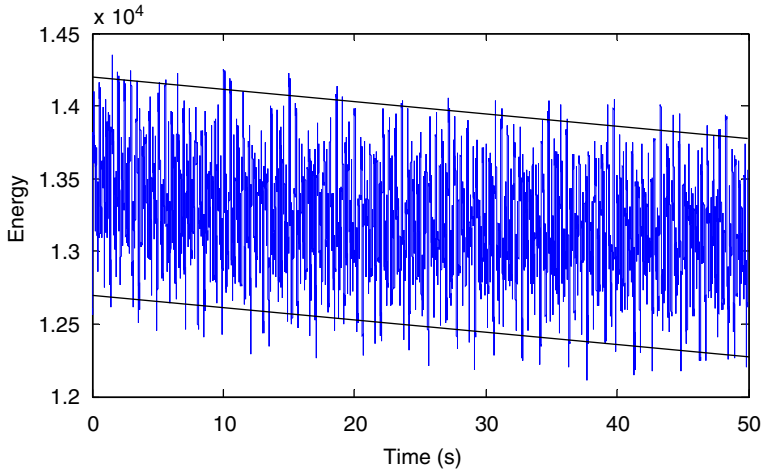

Fig. 7. The total energy of the system computed by RKM with step-size 0.0001.

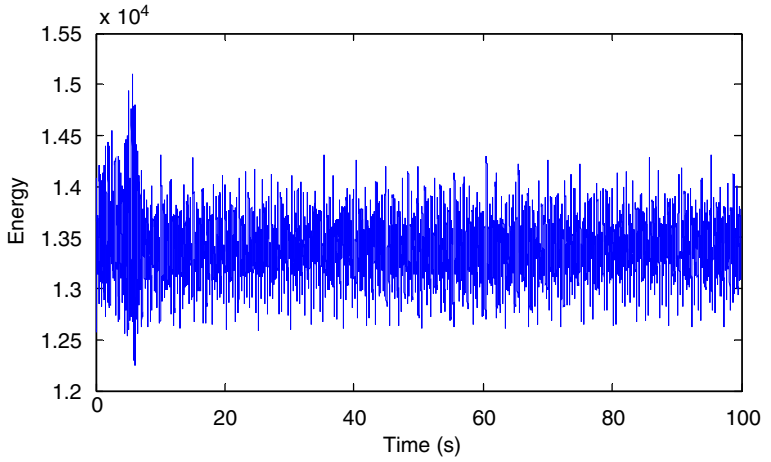

Fig. 8. The total energy of the system computed by SRKM with step-size 0.0005.

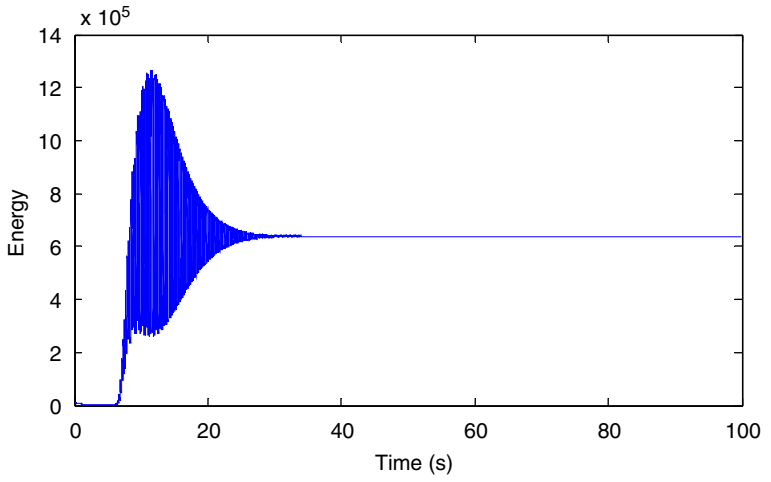

Fig. 9. The total energy of the system computed by RKM with step-size 0.0005.

RKM will continue deviating from the original energy. When the simulation time is long enough, the states maybe converge to zero.

Figs. 8 and 9 show the results of SGA and RKM with time-step 0.0005, respectively. It can be noted from these results that SGA can keep conservation all the same, but the traditional RKM cannot get the real results in a long span of time. By comparing Fig. 9 with Fig. 8, it can be concluded that SGA is subjected to less influence of the step-size than the traditional RKM.

The dynamic model has been established in the framework of Hamiltonian, and SGA has been applied firstly into such a rotating rigid–flexible coupled system. On view of the long periods of time, SGA can maintain the stability of the numerical simulation, and can conserve the total mechanical energy, however, RKM does not.

6.2. High–low frequencies mixed system—the accuracy of solving stiff equations

In order to validate the accuracy of SPIM, a set of stiff differential equations are adopted to be solved by SPIM, PIM and RKM, respectively. Hamiltonian of this system is

$$\Upsilon = \tfrac{1}{2}m_1\dot{x}_1^2 + \tfrac{1}{2}m_2\dot{x}_2^2 + \tfrac{1}{2}m_3\dot{x}_3^2 + \tfrac{1}{2}k_1x_1^2 + \tfrac{1}{2}k_2x_2^2 + \tfrac{1}{2}k_3x_3^2. \tag{48}$$

Then we can get the canonical equation

$$\begin{bmatrix}\dot{\mathbf{q}}\\ \dot{\mathbf{p}}\end{bmatrix} = \begin{bmatrix}0 & \mathbf{M}\\ \mathbf{K} & 0\end{bmatrix}\begin{bmatrix}\mathbf{q}\\ \mathbf{p}\end{bmatrix}, \tag{49}$$

where position vector $\mathbf{q} = [x_1, x_2, x_3]^{\mathrm{T}}$, and momentum vector $\mathbf{p} = [m_1\dot{x}_1, m_2\dot{x}_2, m_3\dot{x}_3]^{\mathrm{T}}$,

$$\mathbf{M} = \begin{bmatrix}1/m_1 & 0 & 0\\ 0 & 1/m_2 & 0\\ 0 & 0 & 1/m_3\end{bmatrix},\ \mathbf{K} = -\begin{bmatrix}k_1 & 0 & 0\\ 0 & k_2 & 0\\ 0 & 0 & k_3\end{bmatrix}.$$

Supposed that $m_1 = 0.1$, $m_2 = 10$, $m_3 = 1000$, $k_1 = 100$, $k_2 = 10$, $k_3 = 1$, then we can gain the analytical solution

$$\begin{bmatrix}x_1\\ x_2\\ x_3\end{bmatrix} = \begin{bmatrix}\sqrt{10}/5 & 0 & 0\\ 0 & 1/5 & 0\\ 0 & 0 & \sqrt{10}/50\end{bmatrix}\begin{bmatrix}\sin(10\sqrt{10}t)\\ \sin(t)\\ \sin(\sqrt{10}/100t)\end{bmatrix} \quad \text{and} \quad \begin{bmatrix}p_1\\ p_2\\ p_3\end{bmatrix} = 2\begin{bmatrix}\cos(10\sqrt{10}t)\\ \cos(t)\\ \cos(\sqrt{10}/100t)\end{bmatrix}. \tag{50}$$

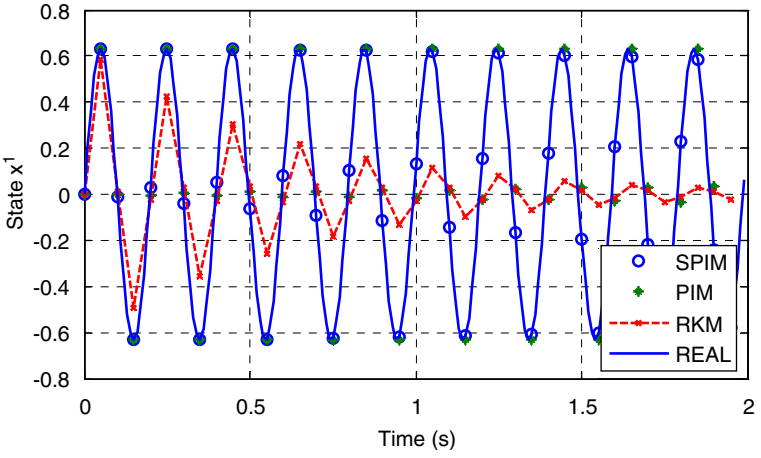

Fig. 10. Results of state x_1 calculated by SPIM, PIM, RKM, and analytical solution (REAL) with step-size 0.05.

The results of state x_1 plotted in Fig. 10 are calculated by SPIM, PIM, RKM, and analytical solution with step size 0.05, respectively. That the result calculated by RKM departs far from the analytical solution has been appeared in Fig. 10. The result calculated by SGA can capture the analytical solution, although there is some error. The result calculated by SPIM can capture accurately the analytical solution, and cannot be observed any difference between the results from SPIM and analytical solution. The errors between the result of SPIM and the analytical solution is displayed in Fig. 11, from which it can be observed that the max error is only 6.1×10^{-15}. From these comparisons, it is concluded that SPIM is a very precise method and its accuracy is far higher than the other two methods.

When the time-step is finished, the results of state x_1 are showed in Fig. 12. From this figure, it can be observed that the results calculated by the four methods are close so much as to superpose entirely. After the errors between three numerical results and analytical solution are studied, big difference between SPIM and the other two numerical method will be found. All these errors are plotted in Figs. 13–15, from which SPIM is proved that it is much better than the other two methods. In the first 2 s, the largest error of SPIM is 3.4×10^{-15}, but that of PIM is 5.4×10^{-4}, and that of RKM is 3.2×10^{-3}. Comparing the results calculated by SPIM with 0.01 and 0.05, we can find SPIM subjects little infection of time-step.

An SPIM has considered the effect of accumulated error, so this algorithm can get the high-accuracy results with large time-step. Simulations will be speeded up by enlarging time-step.

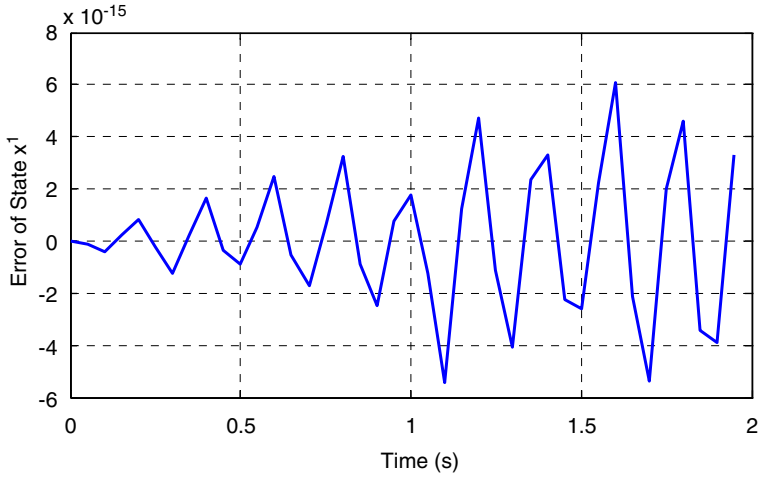

Fig. 11. The error between analytical solution and SPIM with time-step 0.05.

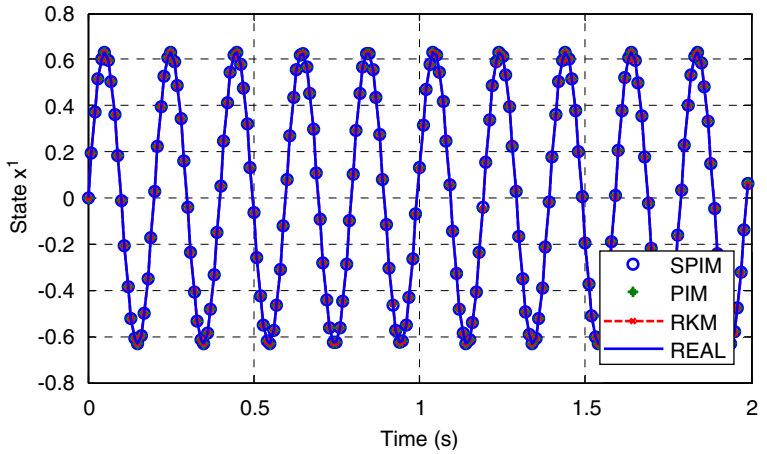

Fig. 12. Results of state x_1 calculated by SPIM, PIM, RKM, and analytical solution (REAL) with step-size 0.01.

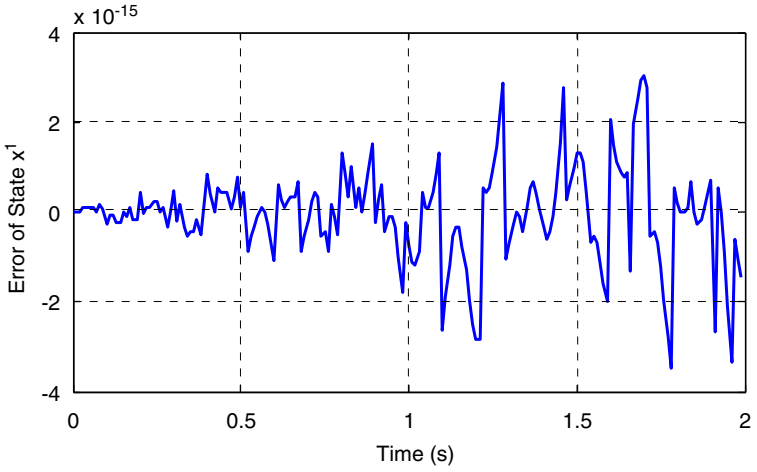

Fig. 13. The error between analytical solution and SPIM with time-step 0.01.

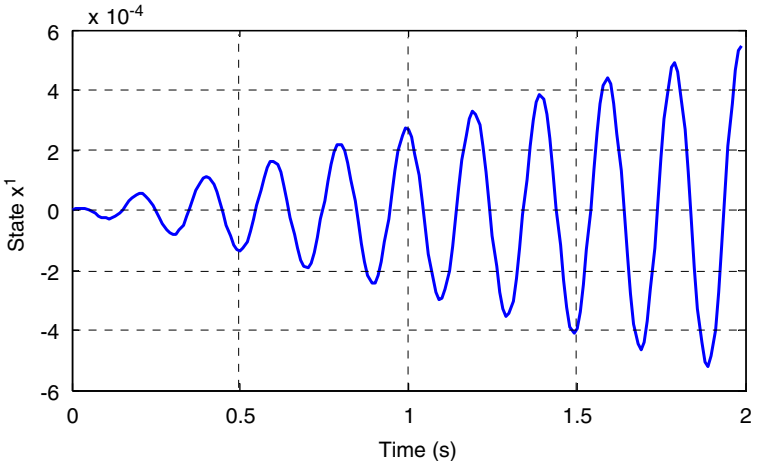

Fig. 14. The error between analytical solution and PIM with time-step 0.01.

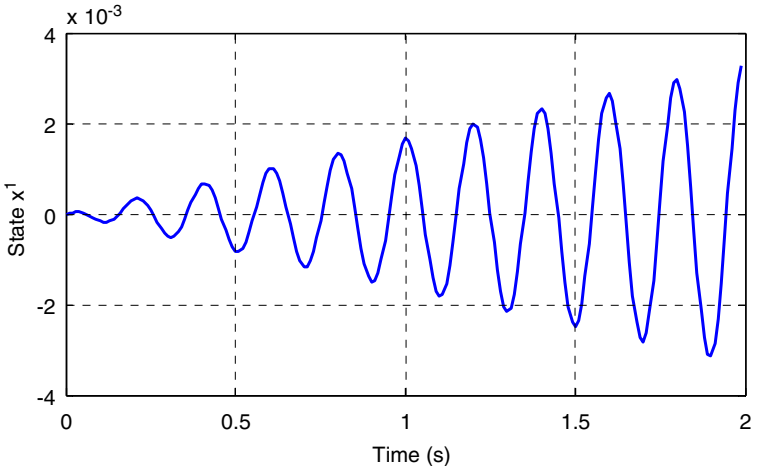

Fig. 15. The error between analytical solution and Runge–Kutta with time-step 0.01.

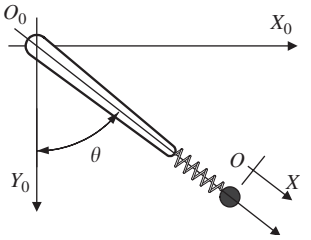

Fig. 16. Structure of compound pendulum.

6.3. Compound pendulum—the ability of solving nonlinear equations

In order to display the ability of solving nonlinear equations, the compound pendulum system is adopted and modeled as a nonlinear system. Parameters of the compound pendulum are listed as follows: the mass of pendulum is $M = 1\,\text{kg}$, and the length of pendulum is $L = 1\,\text{m}$, and the mass of particle is $m = 0.1\,\text{kg}$, and the stiffness of spring is $k = 100\,\text{N/m}$, and $g = 9.81914\,\text{m/s}^2$ is the gravity at latitude 40° north. The initial states are $x_0 = 0.1\,\text{m}$, $\theta_0 = \pi/6$, $p_x(0) = 0$ and $p_\theta(0) = 0$. The structure is shown in Fig. 16.

The total kinetic energy is

$$T = \tfrac{1}{2}(I + J)\dot{\theta}^2 + \tfrac{1}{2}m\dot{x}^2. \tag{51}$$

The total potential energy is

$$V = \frac{1}{2}MgL(1 - \cos\theta) + mg\left(L + x_0 + \frac{mg}{k} - \left(L + x_0 + \frac{mg}{k} + x\right)\cos\theta\right) + \frac{1}{2}k\left(\frac{mg}{k} + x\right)^2. \tag{52}$$

The generalized displacements and generalized momentums are

$$\begin{Bmatrix} x \\ \theta \end{Bmatrix} \text{ and } \begin{cases} p_x = \dfrac{\partial(T - V)}{\partial\dot{x}} = m\dot{x} \\ p_\theta = \dfrac{\partial(T - V)}{\partial\dot{\theta}} = (1 + J)\dot{\theta} \end{cases}, \tag{53}$$

where

$$I = \frac{1}{3}ML^2, \quad J = m\left(x_0 + \frac{mg}{k} + x\right)^2.$$

Then the canonical equations of the system can be written as

$$\begin{bmatrix} \dot{x} \\ \dot{\theta} \\ \dot{p}_x \\ \dot{p}_\theta \end{bmatrix} = \begin{bmatrix} \dfrac{1}{m}p_x \\ \dfrac{1}{I + J}p_\theta \\ \dfrac{m\left(L + \frac{mg}{k} + x\right)}{(I + J)^2}p_\theta^2 - kx + mg\cos\theta \\ -\left[\dfrac{ML}{2} + m\left(L + \frac{mg}{k} + x\right)\right]g\sin\theta \end{bmatrix}. \tag{54}$$

Define approximately

$$\frac{1}{I + J} \approx I - m\left(L + x + \frac{mg}{k}\right)^2 + \left(m\left(L + x + \frac{mg}{k}\right)^2\right)^2 - \left(m\left(L + x + \frac{mg}{k}\right)^2\right)^3$$

and

$$\sin\theta \approx \theta - \frac{1}{6}\theta^3 + \frac{1}{120}\theta^5,$$

then we can get equations, whose form is like as Eq. (32):

$$\dot{\mathbf{z}} = \mathbf{H}\mathbf{z} + \mathbf{F}, \tag{55}$$

where

$$\mathbf{z} = \left[x\ \theta\ p_x\ p_\theta\right],$$

$$\mathbf{H} = \begin{bmatrix} 0 & 0 & \frac{1}{m} & 0 \\ 0 & 0 & 0 & \frac{1}{I + m\left(L + \frac{mg}{k}\right)^2} \\ -k & 0 & 0 & 0 \\ 0 & -\left[\frac{ML}{2} + m\left(L + \frac{mg}{k}\right)\right]g & 0 & 0 \end{bmatrix},$$

$$\mathbf{F} = \begin{bmatrix} 0 \\ \frac{1}{m\left(L + x + \frac{mg}{k}\right)^2} - \frac{1}{I + m\left(L + \frac{mg}{k}\right)^2} \\ \frac{m\left(L + \frac{mg}{k} + x\right)}{(I + J)^2} p_\theta^2 + mg\cos\theta \\ -gx\theta + \frac{1}{6}\left[\frac{ML}{2} + m\left(L + \frac{mg}{k} + x\right)\right]g\theta^3 - \frac{1}{120}\left[\frac{ML}{2} + m\left(L + \frac{mg}{k} + x\right)\right]g\theta^5 \end{bmatrix}.$$

The results plotted in Figs. 17 and 18 are calculated by RKM with time-step 0.0001 and SPIM with time-step 0.01. From these figures, it can be observed that the two kinds of method get close results with different time-steps which are time-step 0.0001 for RKM and time-step 0.01 for SPIM. But the calculation time of

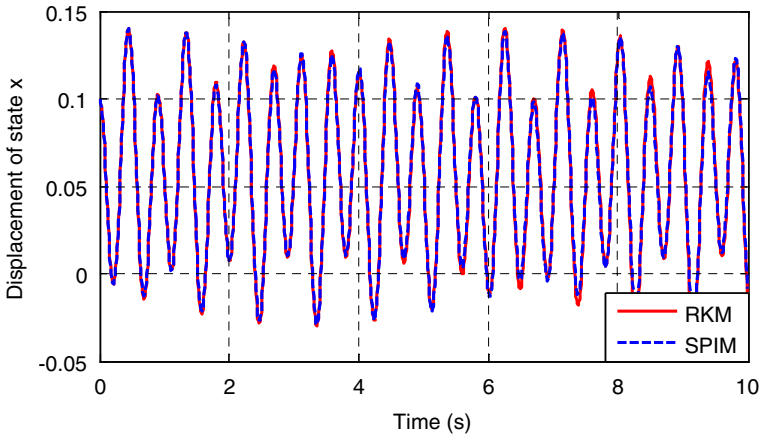

Fig. 17. State x calculated by RKM with time-step 0.0001 and SPIM with time-step 0.01.

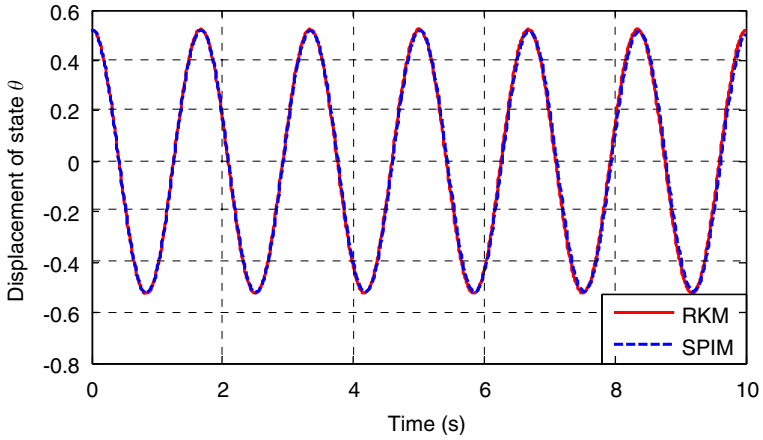

Fig. 18. State θ calculated by RKM with time-step 0.0001 and SPIM with time-step 0.01.

RKM is 753.375 s, and that of SPIM is only 0.079 s. When the time-step of RKM is also 0.01, its accuracy will fall, and the calculated time is still 0.656 s. The calculation time is the average of ten times' calculation.

When SPIM takes time-step 0.01, in order to meet the same accuracy, RKM has to take time-step 0.0001. The time-step of SPIM is 100 times of that of RKM, and the calculation time of SPIM is 0.010486% of that of RKM. From these data, it can be proved that the computation efficiency of SPIM is higher than that of RKM.

When the same time-step 0.01 is adopted for SPIM and RKM, the magnitudes of calculation time are 0.079 and 0.656 s, respectively. SPIM is not only higher than RKM in efficiency, but also far more accurate than RKM. It is promising that SPIM is used in simulation of control to solve the real-time problem.

7. Conclusions

This paper investigates a suitable SGA and presents an improved SPIM for the rotating rigid–flexible coupled systems. SPIM has been adopted to analyze different kinds of engineering structures to show the advantages of the stability, the accuracy and the efficiency. Some significant conclusions have been gained as follows:

(1) The coupled model was established by the generalized Hamilton's principle and discretized by the finite element method. And the canonical form of the coupled structure has been gained by canonical transformations. Most structures can be abstracted from this model, and which can be adopted to analyze the highly flexible structures.
(2) A suitable SGA has been formulated to solve rotating rigid–flexible coupled systems. And it has been proven that SGA cannot only solve this coupled system, but has higher stability than the traditional RKM. It is the first time to apply the SGA to solving such a coupled model.
(3) SPIM, which integrates not only the computational stability which is the characteristic of the SGA, but also the accuracy of PIM, has been established by introducing the idea of PIM into SGA. The results calculated by SPIM can ensure the stability and the accuracy at the same time. So we can enlarge the time-step to speed up the computation.
(4) It has been proven from these simulations SPIM can be used to solve the nonlinear systems successfully. Meanwhile, it can be used to speed up the computation by enlarging time-step.
(5) Three different kinds of examples were adopted to prove SPIM cannot only solve the nonlinear and stiff equations, but improve the computational efficiency. It is a promising method to deal with the real-time problems in control field, or to speed up the calculations in computer.

Acknowledgments

The authors are grateful for supports from the National Natural Science Foundation of China (10572119), the Program for New Century Excellent Talents in University (NCET-04-0958), the Natural Science Foundation of Henan province in China (0511011800), and the Open Foundation of State Key Laboratory of Structural Analysis of Industrial Equipment.

References

[1] K. Feng, On difference schemes and simplectic geometry. in: K. Feng (Ed.), *Proceedings of the 1984 Beijing Symposium on Differential Geometry and Differential Equations*, Science Press, Beijing, 1985, pp. 42–58.
[2] R.D. Ruth, A canonical integration technique, *IEEE Transactions on Nuclear Science* 30 (1983) 26–69.
[3] K. Feng, M.Z. Qin, Hamiltonian algorithms for Hamiltonian dynamical systems, *Progress in Natural Science* 1 (2) (1991) 106–116.
[4] K. Feng, M.Z. Qin, Hamiltonian algorithms for Hamiltonian systems and a comparative numerical study, *Computer Physics Communications* 65 (1991) 173–187.
[5] D.G. Andrews, *An Introduction to Atmospheric Physics*, Cambridge University Press, Cambridge, 2000.
[6] J.A. Izaguirre, S. Reich, R.D. Skeel, Longer time steps for molecular dynamics, *Journal of Chemical Physics* 110 (1999) 9853–9864.
[7] Q. Wang, K.L. Huang, Q.S. Lu, Symplectic Algorithm for Hamilton Multibody System, *Chinese Journal of Computational Physics* 14 (1) (1997) 35–39 (in Chinese).
[8] S.R. Buss, Accurate and efficient simulation of rigid-body rotations, *Journal of Computational Physics* 164 (2) (2000) 377–406.
[9] A.Y.T. Leung, S.G. Mao, A symplectic Galerkin method for non-linear vibration of beams and plates, *Journal of Sound and Vibration* 183 (3) (1995) 475–491.
[10] W.X. Zhong, On precise integration method, *Journal of Computational and Applied Mathematics* 163 (2004) 59–78.
[11] T. Belytschko, W.K. Liu, B. Moran, *Nonlinear Finite Elements for Continua and Structures*, Wiley, New York, 2000.
[12] K. Feng, M.Z. Qin, *Symplectic Geometric Algorithms for Hamiltonian Systems*, Zejiang Science and Technology Press, 2003 (in Chinese).
[13] K. Dekker, J.G. Verwer, *Stability of Runge–Kutta Methods for Stiff Nonlinear Differential Equations*, North-Holland, Amsterdam, New York, 1984.
[14] Z.C. Deng, W.X. Zhong, Time precise integration method for constrained nonlinear control system, *Applied Mathematics and Mechanics* 23 (1) (2002) 16–22.